

Molecular Structure of $\text{Si}_x\text{Te}_{1-x}$ Glasses and Oxygen Alloying Effects

P. Boolchand, B. Norban, R.ENZWEILER

Department of Physics and Department of Electrical and
Computer Engineering, University of Cincinnati
Cincinnati, Ohio 45221-0030

and

J.E. Griffiths and J.C. Phillips

A. T. and T. Bell Laboratories
Murray Hill, New Jersey 07974

ABSTRACT

Raman vibrational modes, Mössbauer Electric Field Gradients and crystallization temperatures exhibit threshold behavior near the composition $x=0.20$ in binary $\text{Si}_x\text{Te}_{1-x}$ glasses. This threshold is evidence of a morphological structural change that may be driven by average coordination number. At $x \leq 0.20$, the glass structure largely consists of Te_n chain segments cross-linked by Si atoms and this structure is characteristic of other IV-VI semiconductors. At $x \geq 0.20$, Te_n chains reconstruct with tetrahedral $\text{Si}(\text{Te}_{1/2})_4$ units and nucleate a defect-ridden Si_2Te_3 -like closed packed layer structure which is more metallic in character. Oxygen alloying effects in the semiconducting phase are qualitatively different from those in the metallic phase. The presence of oxygen drastically alters the kinetics of crystallization of the alloy glasses.

1. INTRODUCTION

Glassy alloys of Si and Ge with either oxygen or chalcogens (S, Se and Te) form an important class of electronic materials. A multiprong experimental effort spanning the past two decades has been expended to decode the atomic scale structure of these alloys¹. Raman scattering², diffraction³, scanning calorimetry and more recently spin resonance, Mössbauer spectroscopy⁴ and high resolution electron-microscopy⁵ have played increasingly important roles in understanding the morphological structure of these technologically important materials. For the case of Si- and Ge- chalcogenides, there is convincing evidence⁴ to suggest that the atomic scale structure of glasses, both short-range ($\sim 2\text{\AA}$) as well as medium range ($\sim 30\text{\AA}$) bears a close resemblance to that of corresponding crystals. Exceptions to this general rule (also called as the Ioffe-Regel rule) do occur and can be traced to the presence of low-pressure molecular conformations present in a glass network which are unstable against compaction in the corresponding crystalline network.⁶

Recent Raman scattering⁷ and inelastic neutron scattering⁸ results on SiS_2 and SiSe_2 have decisively shown that the medium range order in these glasses is dominated by fragments of edge-sharing tetrahedral chains some of which are locally parallel to each other as found in corresponding crystals, while others are a random variant giving rise to cross-linking of chains by corner-sharing tetrahedra. Similar models based on large crystal-like molecular fragments also appear to be rather successful in understanding new Mössbauer spectroscopic results⁹ on the Ge-chalcogenides. These site-specific results have been particularly insightful in determining the size of characteristic molecular fragments by fixing the surface to volume ratio. These new ideas on glass structure are in sharp contrast to the totally random models¹ often invoked in the late sixties and early seventies to explain diffraction results on these materials.

While not as extensive as in the $\text{Si}_2(\text{S or Se})_{1-z}$ binaries, bulk glass formation in the $\text{Si}_x\text{Te}_{1-x}$ binary does occur over a substantial Si concentration range $0.10 < x < 0.27$ about the eutectic composition $x_e=0.17$ as noted by Cornet¹⁰ several years ago. These results are of special interest because in the equilibrium phase diagram, a Si crystalline compound occurs only at $z=1/3$ stoichiometry with the lighter chalcogens (S, Se) but at $x=2/5$ stoichiometry with the heavier chalcogen (Te). Furthermore, these crystals have widely different molecular structures: $\text{Si}(\text{S or Se})_2$ consists of linearly polymerized infinitely long and parallel chains of edge-sharing $\text{Si}(\text{S}_{1/2} \text{ or } \text{Se}_{1/2})_4$ tetrahedra¹¹ giving rise to a semiconductor; while Si_2Te_3 forms a more metallic structure based on closed-packed arrays of Te-layers in which $2/3$ rds of the octahedral cages are occupied by Si_2 dimers.¹²

Basic and applied interest in the molecular structure of the present glasses also derives from the idea of rigidity percolation^{13,14}. In covalent glassy networks constrained by bond-bending and bond-stretching forces, the existence of mechanical thresholds were recently predicted by Phillips¹³ and Thorpe¹⁴ as a function of average coordination number (CN). These workers independently showed that when the $\langle \text{CN} \rangle = 2.40$ such a covalent network sits at a mechanical critical point, in which rigid regions

percolate in a mean field sense. These ideas provide a natural basis to understand the existence of threshold behavior in Raman vibrational modes, Mössbauer Electric Field Gradients and crystallization temperatures near the composition $x=0.20$ in the present glasses. $\text{Si}_x\text{Te}_{1-x}$ glasses near $x \approx 0.10$ predominantly consists of Te_n chains cross-linked by Si sites. As x approaches 0.20 from below, Te_n chains rapidly reconstruct with $\text{Si}(\text{Te}_{1/2})_4$ units to nucleate Si_2Te_3 -like fragments in the composition range $0.10 \leq x \leq 0.20$. The compacted Si_2Te_3 -like fragments grow progressively larger in size with x as these first percolate near $x \approx 0.20$. At $x \geq 0.30$, the Si_2Te_3 fragments suppress glass formation by spontaneously crystallizing unless fast quench ($\geq 10^3$ K/s) rates are used to kinetically freeze these large fragments.

Particularly revealing are oxygen alloying effects in the present binary glasses. We have found that oxygen is easily alloyed in both the floppy (particularly at $x \approx 0.10$), and the rigid fragments (i.e. when $x > 0.20$). Oxygen alloying of $\text{Si}_x\text{Te}_{1-x}$ glasses produces remarkable changes in the mechanical properties, crystallization behavior, glass transition temperatures, semiconductor to metal transition pressures. Conceivably these effects may play an important role in technological applications of these materials.

2. EXPERIMENTAL CONSIDERATIONS

The elements in the desired proportion were sealed in 5mm id fused quartz ampules at a pressure of 5×10^{-7} Torr using a CTI cryopump based vacuum system. The melts typically 0.5gm in size, were held at a 1000°C for 5 days in a vertical configuration and periodically shaken to homogenize before quenching in water. This procedure yielded homogeneous glassy samples in the composition range $0.10 < x < 0.25$ that displayed reproducible glass transition $T_g(x)$ and crystallization temperature $T_c(x)$. Oxygen doping of the samples was achieved by using traces of TeO_2 as a starting material in conjunction with elemental Si and Te and alloying done both in vacuum or a 300mm partial pressure of high purity argon¹⁵. Typical concentrations of oxygen in the samples were 1/2 at % although this was not established directly.

Differential scanning calorimetry traces, taken with a Perkin-Elmer Model 2C instrument, displayed two distinct crystallization temperatures, T_{c1} and T_{c2} at $x < 0.20$ but only one crystallization temperature at $x \geq 0.21$. Figure 1 displays the compositional dependence of $T_g(x)$, $T_{c1}(x)$ and $T_{c2}(x)$ taken at a 20K/min scan rate.

Raman scattering from the bulk glass chips were obtained using the 7525Å exciting line from a Kr-ion laser. Spectra were recorded as a function of laser power to understand the various steps leading to photocrystallization both at $x < 0.20$ and at $x > 0.20$. Details of the experimental set up are described elsewhere¹⁶. Figures 2a and 2b reproduce spectra observed at $x=0.18$ and 0.23. Reference spectra of crystals in this binary (c-Te and c- Si_2Te_3) were also obtained for purposes of comparison.

¹²⁵Te Mössbauer spectra of the glasses were taken at 4.2K using a source of 58 days ¹²⁵Te^m in cubic GeTe¹⁷. Spectra of the glasses display a quadruple doublet whose splitting (Δ) decreases with x in a systematic fashion to display a cusp at $x=0.20$ shown in Figure 3. Spectrum of c- Si_2Te_3 was also studied for reference purposes. ¹²⁹I Emission spectra of the glasses and of c- Si_2Te_3 were also studied and will be discussed elsewhere.

3. DISCUSSION OF RESULTS AND GLASS MOLECULAR STRUCTURE

3.1. Differential scanning calorimetry

Several years ago Cornet¹⁰ found that the compositional dependence of glass transition temperatures $T_g(x)$ and first crystallization temperatures $T_{c1}(x)$ in binary $\text{Si}_x\text{Te}_{1-x}$ glasses is linear in the composition range $0.10 \leq x \leq 0.25$. Our results confirm the linear variation of $T_g(x)$ and $T_{c1}(x)$ found earlier by Cornet. These results do differ qualitatively from those of Asokan, Parthasarathy and Gopal¹⁸, however, who observe a local minimum in both $T_g(x)$ and $T_{c1}(x)$ at $x=0.20$. The T_g differences between our results and those of Asokan et al. are summarized in Figure 4 and arise due to oxidation of their samples and is a point we return to in section 4.

Particularly noteworthy in our scans¹⁹ is the existence of two crystallization temperatures T_{c1} and T_{c2} at $x < 0.21$ but only one crystallization exotherm at $x \approx 0.21$. Similar homogeneous behavior in crystallization temperatures of these glasses above the threshold composition x_c is also observed by Asokan et al. on their samples¹⁸. We have also carried out these calorimetric experiments at a much small scan rate of 5K/min and find that the threshold composition of $x_c \approx 0.20$ is not altered although the absolute values of T_{c1} and T_{c2} are systematically lowered. Clearly the existence of the threshold composition $x_c = 0.20$ is not a kinetic phenomenon associated with the crystallization process but must have a structural origin.

We identify¹⁹ the temperature T_{c1} with crystallization of the "floppy part" of the glass network i.e. amorphous Te, to form c-Te, while the temperature T_{c2} is associated with crystallization of the rigid Si-containing cross links to form c- Si_2Te_3 . The floppiness of the amorphous Te network derives from both chemical as well as topological

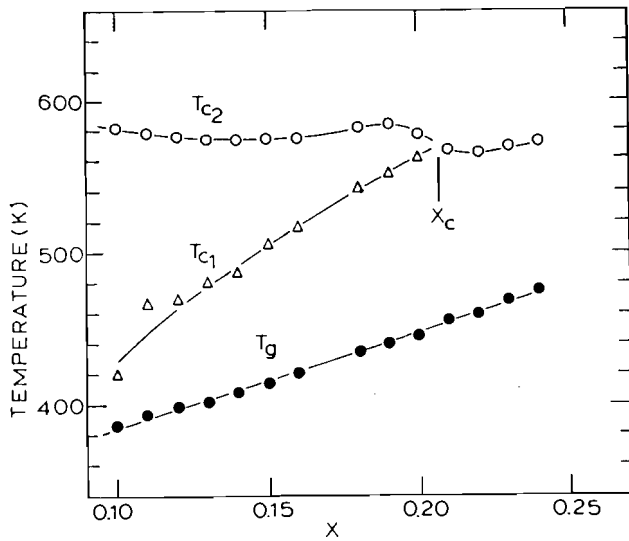


Figure 1. Glass (T_g) and crystallization (T_c) temperatures of Si_xTe_{1-x} glasses plotted as a function of x . A scan rate of 20K/min, a range setting of 5 and 20 mgrams mass of the crushed glass sample was used in a Perkin-Elmer model 2C instrument for these scans.

Figure 2a. Raman spectra of $Si_{18}Te_{82}$ glass taken as a function of laser power in mW at 7525Å: A.21, B.32, C.45, D.64, E.10. Power was reduced to 10mW for 30 min. after D before scanning to record E. Asteriks indicate laser plasma lines. For other details see ref. 19.

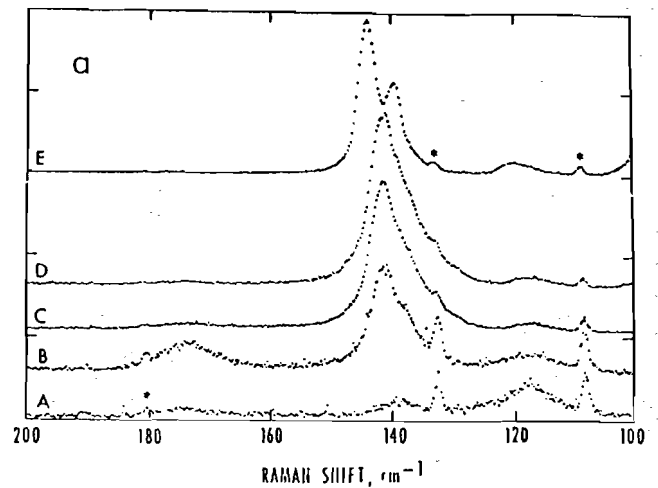
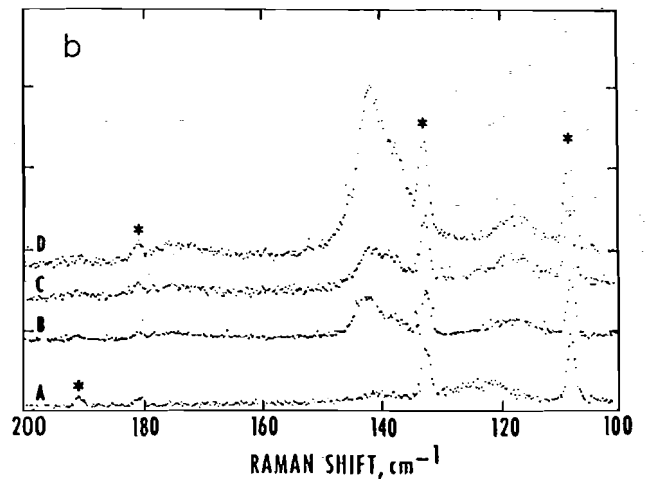


Figure 2b. Raman spectra of $Si_{23}Te_{77}$ glass as a function of laser power in mW at 7525Å: A.6.4, B.16, C.19.3, D.28.5.



considerations. The former is due to the large mass and low melting point of Te ($m_{Te}=127$) in relation to Si ($M_{Si}=28$) and leads to Te-Te bonds being the softest chemical bonds of the network. The low coordination number of Te ($m=2$) on the other hand represents the topological factor contributing to the floppiness of the amorphous Te network. The first step toward crystallization of Te-rich binary $Te_{1-x}Z_x$ glasses ($Z=Si, Ge, Al, Ga, \dots$) is the splitting off^{9,10} of trigonal Te_n chains leaving a glass residue that is enriched in Z and understandably is characterized¹⁸ by a higher T_g than the virgin glass. Above the threshold i.e. $x > 0.20$, the occurrence of a unique crystallization temperature, may be explained by the coalescing of the $Si(Te_{1/2})_4$ units with the excess Te (in the chain fragments) to nucleate a new rigid molecular fragment based on closed packed layers of Te in which Si_2 units are inserted. The linear variation of $T_g(x)$ observed in the present glasses is quite similar to a variation reported earlier in As-S²⁰ and Ge-Sn-S glasses²¹. These results are consistent with the idea that even these simple binary glasses are not homogeneous on a microscopic scale and that molecular phase separation in these glasses occurs intrinsically on a scale of 30Å or so.

3.2. Raman scattering

Our Raman scattering results on $Si_{18}Te_{82}$ glass (Fig. 2a) at the lowest power (spectrum A, 21mW) display three broad peaks at 118 cm^{-1} , 138 cm^{-1} , and 173 cm^{-1} . The two lowest frequency modes can be attributed²² to disordered chains of Te which are either phase-separated by photon-induced bond cleavage or are connected at one end of each chain to structural elements existing in the glass. Analogous phonon frequencies for ordered chains (Te_n) in c-Te are known²² to occur at 123 and 143 cm^{-1} . Dramatic changes begin to evolve at higher powers (B-D). The peak at 173 cm^{-1} rapidly grows in strength in B and almost completely band shape continues to grow from B through D with peak frequency of about 141 cm^{-1} . These changes appear to indicate the existence of $SiTe_3$ face-sharing tetrahedra emerging in the glasses. Such tetrahedra are known to occur in c- Si_2Te_3 ²³. One also notes that the nature of the peak near 120 cm^{-1} changes its position and shape as the bulk glass in the scattering volume evolves toward a $SiTe_3$ composition.

Several comments can be made on the microscopic origin of the 173 cm^{-1} mode. This mode does not arise from elemental Te nor is it observed in the spectrum of c- Si_2Te_3 . A reasonable candidate is clusters composed of $SiTe_{4/2}$ tetrahedral units which intrinsically occur in the virgin glass as revealed by the presence of this band in spectrum A. Laser irradiation at a 32mW power level (spectrum B, Fig. 2a) significantly enhances the signal strength of the 173 cm^{-1} band probably because cleaving of Te_n chains blue shifts the optical absorption edge and leaves a Si-rich bulk glass in which metastable clusters of tetrahedral $SiTe_{4/2}$ units predominate. At still higher level, these clusters reconstruct with the cleaved Te_n chains to nucleate Si_2Te_3 crystals which display¹⁵ the narrow but intense band at 145 cm^{-1} . These results also show the metastable character of the $SiTe_{4/2}$ units present in the glass. Such tetrahedral units apparently do not occur in a crystalline form as revealed by the absence of a stable crystalline compound of $SiTe_2$ stoichiometry²³.

One may estimate the expected vibrational frequencies of possible ($SiTe_{4/2}$) structural units by comparison with the frequencies of similar structures in SiS_2 and $SiSe_2$ glasses in which both edge and corner sharing tetrahedra are known²⁴ to exist. The observed peak frequency values for appropriate bands in these glasses and for Si_xTe_{1-x} are scaled by the ν_1 frequencies in $SiCl_4$, $SiBr_4$ and SiI_4 to compensate changes in the reduced masses of the oscillators. These calculations¹⁹ suggest that the band at 173 cm^{-1} arises from a stretching mode probably originating in edge sharing tetrahedra.

After spectrum D was recorded at a power level of 64 mW, the incident power was reduced to 10 mW for 30 minutes before scanning E at that power. This significantly reduces the optical and thermal energy input to the sample and allows cooling and crystallization to occur with the formation of c- Si_2Te_3 as is evident in E. The scattering cross section of Si_2Te_3 is so large compared to other species that it dominates the observed spectrum. In the dark, over a period of 17 h at room temperature, crystallization is partially reversed but the spectrum of c- Si_2Te_3 can still be observed. Its intensity relative to E is reduced by a factor of about 50. The surface of the sample, however, has suffered observable damage. Melting is indicated and is consistent with the observations in spectra D and E.

Samples with $x > 0.20$ behave under the influence of laser irradiation in much the same way as those with $x < 0.20$ with one main exception. The amplitude of the 173 cm^{-1} band is much diminished and as the Te/Si ratio decreases, it plays a lesser and lesser role in the convoluted pathway toward crystallization (Fig. 2b). This supports our previous inference that the molecular structure responsible for this band has a composition $x < 0.4$. It is striking that this transitional band appears most strongly for x close to $x=0.18$ which is close to $x_c = 0.20$. Samples with $x = 0.18 \pm 0.02$ show this band more strongly than for samples with $x=0.23$. The structure responsible for this band forms just before x increases to x_c , and may be a precursor to defective Si_2Te_3 .

3.3. Mössbauer spectroscopy

¹²⁵Te Mössbauer spectra of the binary glasses display a partially resolved doublet (Fig. 3a) whose origin is traced^{17,25} to a nuclear quadrupole splitting (Δ) in the $3/2+$

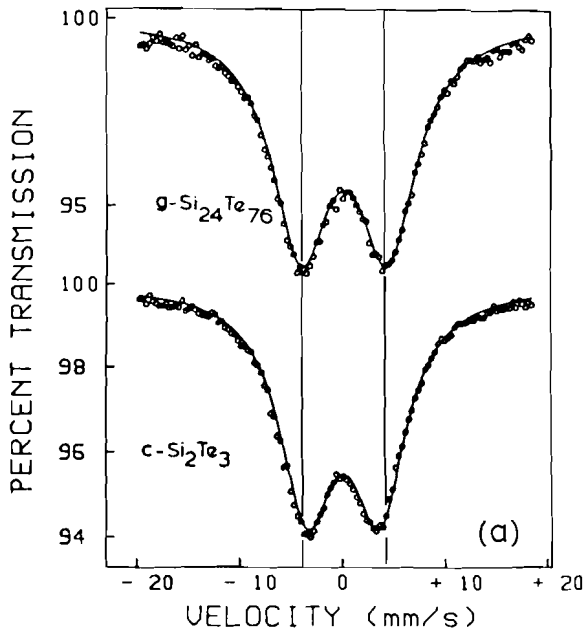


Figure 3a. ^{125}Te Mössbauer spectra of indicated glass and crystal recorded at 4.2K using a source of $^{125}\text{Te}^m$ in c-GeTe.

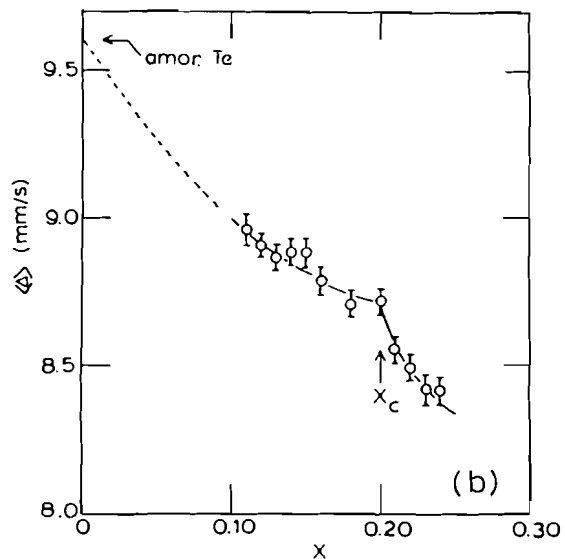


Figure 3b. x -variation of the ^{125}Te quadrupole splitting (Δ) in $\text{Si}_x\text{Te}_{1-x}$ glasses exhibiting a cusp near $x=0.20$.

first excited state. The quadrupole splitting measures the Electric Field Gradient, which in these covalent materials is determined principally by the distribution of electrons in the 5p bonding and non-bonding lone pairs of Te at various sites in the network. Since the natural linewidth of the ^{125}Te resonance of 5.20mm/s is comparable to the quadrupole splittings ($\sim 8\text{mm/s}$) of the Te sites, it is not possible to deconvolute contributions of at least two types of Te sites in these glasses. These sites can be deconvoluted using ^{129}I emission spectroscopy however, and the results are discussed elsewhere. The two sites in question are as follows. One of these sites (site B) represents a Te site that is 2-fold coordinated to Te near neighbors in a Te-chain segment as in a-Te. This site possesses a large $\Delta_B = 9.6\text{mm/s}$ as shown elsewhere¹⁷. The second site (site A) represents a Te site that is 2-fold coordinated to Si near neighbors and this site acts as a bridge between tetrahedral $\text{Si}(\text{Te}_{1/2})_4$ units, with a smaller $\Delta_A \sim 7.3 \text{ mm/s}$.

Starting from a-Te (i.e. $x=0$), we can understand the decline in $\langle \Delta(x) \rangle$ in the composition range $0 \leq x \leq 0.20$ in terms of growth in the Te A site population at the expense of Te B sites, as progressive Si alloying promotes crosslinking of the Te-chain segments. The more rapid decline in $\langle \Delta(x) \rangle$ at $x \geq 0.20$ which leads to the cusp at $x = 0.20$ (Fig. 3b) is signature of more drastic structural changes taking place in the glass network at the mechanical threshold. We can understand the sharp reduction in $\langle \Delta \rangle$ due to a sudden loss in the Te-chain sites as the Te-chain segments rapidly coalesce with the tetrahedral $\text{Si}(\text{Te}_{1/2})_4$ units at $x=0.20$ to nucleate a new molecular fragment. This fragment consists of closed packed layers of Te atoms based on the defect ridden Si_2Te_3 -like layered cluster in which instead of the usual 1/3 Si dimer vacancies, there are more like 2/3 vacancies corresponding to a stoichiometry of SiTe_3 appropriate for $x \approx 0.25$. On chemical grounds this reconstruction appears plausible for several reasons. X-ray crystallographic studies of Ziegler²³ on non-stoichiometric $\text{Si}_{1+y}\text{Te}_3$ crystals show that the closed packed layer structure of Si_2Te_3 exists over a broad range $1/2 < y < 1$ of stoichiometries with dimers statistically missing from Te octahedral cages. In the glasses the free energy of the layered cluster fragments is probably lowered even more than in the crystals as constraints due to long range order are lifted, thus making feasible for the layered fragment to relax and accommodate an even wider range of cation to anion stoichiometries than is possible in the crystals. In our structural model of these glasses the drastic network reorganization taking place at the vector percolation threshold, $x=0.20$, can also be stimulated by a photon pump at $x \leq 0.20$, as revealed by our Raman scattering results discussed earlier in section III c.

4. OXYGEN ALLOYING EFFECTS

First indications that oxygen plays an important role in determining the glass transition temperatures ($T_g(x)$) and mechanical properties of $\text{Si}_x\text{Te}_{1-x}$ glasses particularly when $x < 0.20$ emerge when we compare our $T_g(x)$ results to those of Asokan et al.¹⁸, as shown in Figure 4. The open elliptical circles represent glass transition temperatures of $\text{Si}_x\text{Te}_{1-x}$ glasses prepared by alloying the elements in presumably impure (oxygen

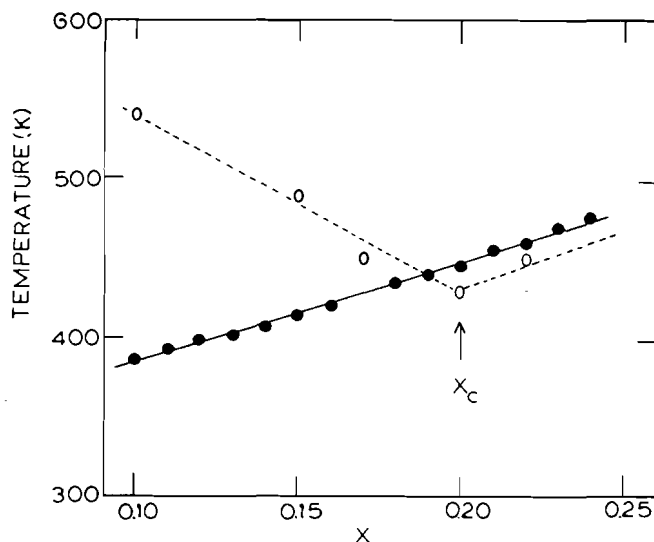


Figure 4. Filled circles and open elliptical circles represent T_g of Si_xTe_{1-x} glasses reported by B. Norban et al. ref. 19 and S. Asokan et al. ref. 18.

containing) argon by Asokan et al. Particularly striking in these results is the fact that oxygen alloying effects are drastic at $x \leq 0.20$ causing T_g 's to increase by nearly 130K at $x=0.10$ for example, with virtually little or no T_g change taking place once the Si concentration $x \geq 0.20$. At $x \geq 0.20$, the role of oxygen is to frustrate crystallization of these glasses and is a point we develop next.

To examine the underlying issue further we have deliberately alloyed oxygen in pure Si_xTe_{1-x} binary glasses and have examined such samples in scanning calorimetry. Figure 5 displays some of the results at a concentration $x=0.10$. At the outset we can state that our attempts to alloy Si and Te in a 300mm partial pressure of high purity argon produces no change in either T_g or T_c from the values characteristic of pure $Si_{10}Te_{90}$ bulk glass i.e. a glass prepared by alloying the material in vacuum (see Fig. 5a). The DSC trace of an oxygen alloyed glass on the other hand (Fig. 5b) displays three new features labelled as T_g' ($\approx 460K$), T_{c1}' ($\approx 600K$) and T_{c2}' ($\approx 670K$). The T_g' endotherm and T_{c1}' and T_{c2}' exotherms mimic the characteristic temperatures of a $Si_{10}Te_{90}$ glass reported by Asokan et al. and lead us to believe that these values are characteristic of an oxygen bearing $Si_{10}Te_{90}$ glass. Figure 5c displays a trace of a $Si_{10}Te_{89.5}O_{0.5}$ bulk glass that was alloyed in a 300mm partial pressure of high purity argon. The principal changes between traces b and c of Figure 5 are that presence of argon in alloying and melt-quenching process promotes growth of the oxygen bearing $Si_{10}Te_{90}$ phase as manifested by the profound increase in the heat of crystallization under exotherms T_{c1}' and T_{c2}' in relation to those under T_{c1} and T_{c2} .

One possible explanation of the large T_g increase (from $T_g=390K$ to $T_g'=480K$) upon oxygen alloying is as follows. Microscopically one may visualize oxygen to terminate Te_n chains and/or to selectively replace Te at internal surfaces of characteristic clusters of the glass network. The interfacial tension in the oxygen dressed clusters is probably enhanced on account of charge transfer effects and shifts to higher values the softening temperature of the glass.

Our final comment pertains to the crystallization kinetics of an argon alloyed $Si_{10}Te_{89.5}O_{0.5}$ glass sample. This is illustrated in figure 6 as a sequence of DSC traces (a-e) taken at 20K/min on the same sample. At the outset one can state that a pure $Si_{10}Te_{90}$ glass completely crystallizes irreversibly after scan a of figure 5. Traces a-d of figure 6 are rather unusual in this respect and suggest that the kinetics of crystallization of the oxygen bearing $Si_{10}Te_{90}$ glass are drastically slowed down. In the first step of crystallization we note that T_{c1} and T_{c2} exotherms kinetically are the fastest ones to evolve, suggesting that both these thermal features are probably related to the floppy part (a-Te) of the network: T_{c1} reflecting crystallization of the pure a-Te clusters while T_{c2} of the oxygen stabilized larger a-Te clusters. We believe that both T_{c2} and T_{c1} exotherms which kinetically are the slowest ones to evolve (see scans b, c and d) relate to crystallization of the rigid molecular fragments and this process is apparently frustrated by the presence of oxygen impurities to obtain c- Si_2Te_3 . We are currently examining these materials in Raman scattering, Infrared reflectance and Mössbauer spectroscopy experiments.

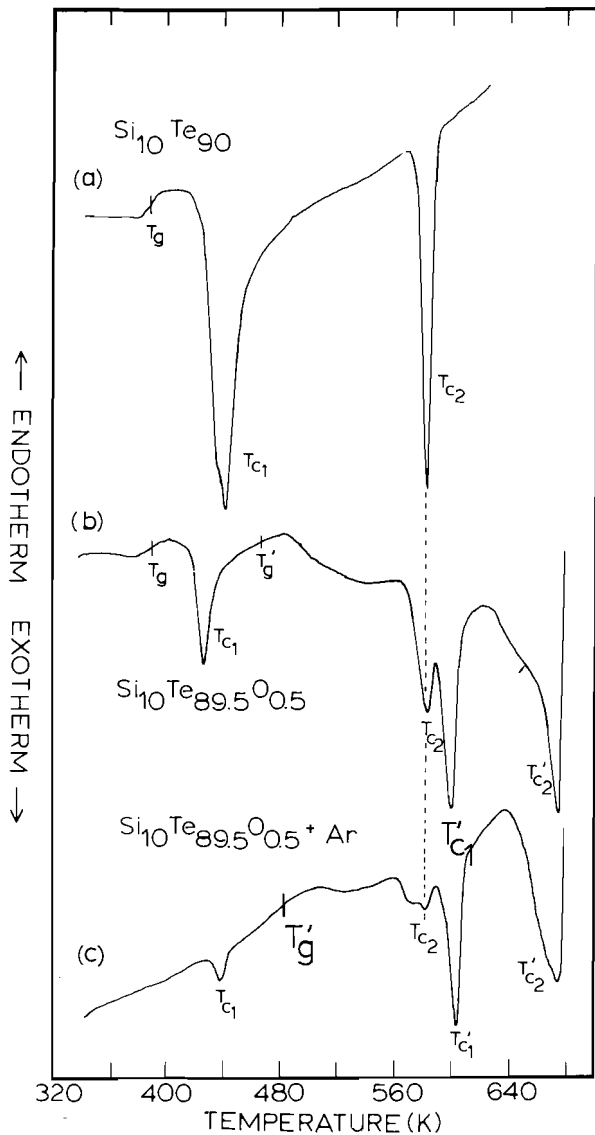


Figure 5. DSC traces of indicated glasses showing new thermal features at T_g' , T_{c1}' and T_{c2}' upon oxygen alloying.

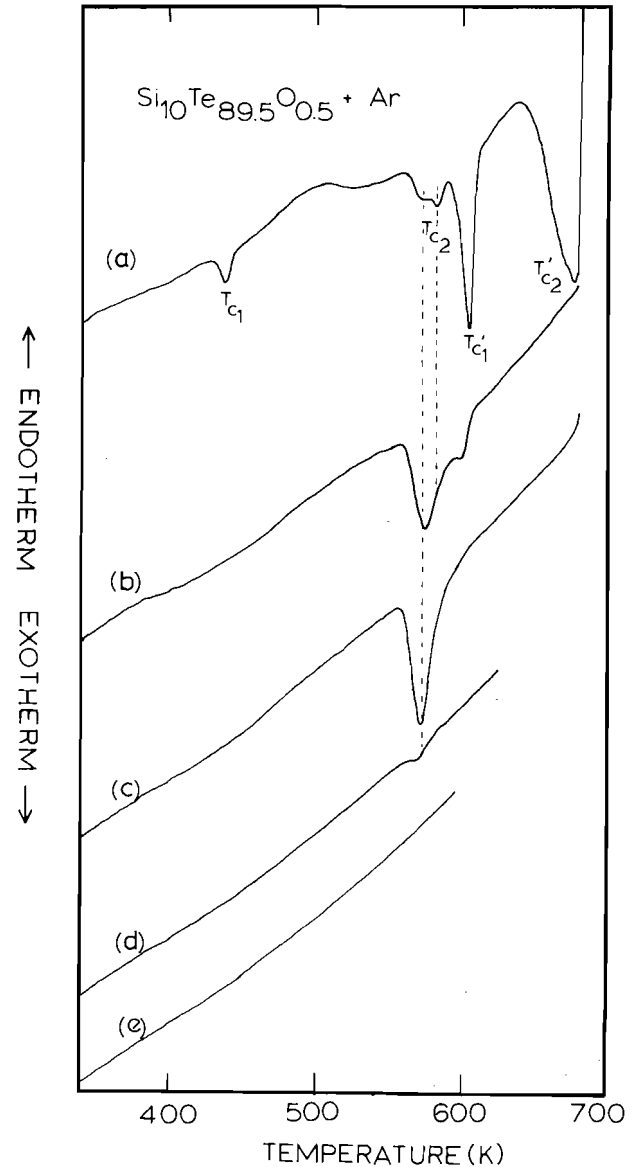


Figure 6. DSC traces of indicated sample taken sequentially a-e at 20K/min. Note the particularly slow kinetics of crystallization associated with T_{c2} and T_{c1}' exotherms, both of which are believed to be related to the formation of $c\text{-Si}_2\text{Te}_3$.

5. CONCLUDING REMARKS

In summary, our scanning calorimetry results, Raman and Mössbauer spectroscopic observations on $\text{Si}_x\text{Te}_{1-x}$ glasses provide evidence of a major structural reorganization taking place at the vector percolation threshold. The proposed structural reorganization provides a natural explanation for several of our observations which include (a) the sharp decline in $\langle \Delta \rangle$ marked by a cusp at $x = 0.20$ (1), (b) the absence of T_{c1} crystallization exotherm associated with Te-chains at $x > 0.20$, (c) the formation of $c\text{-Si}_2\text{Te}_3$ as the final crystalline product upon crystallization of the Si-rich ($x > 0.20$) glasses, and (d) rapid growth in scattering strength of vibrational modes characteristic of microcrystalline- Si_2Te_3 at $x \geq 0.20$. Our structural model could provide a basis to understand the cusp near $x = 0.20$ in the composition dependence of the semiconductor-metal transition pressure observed elsewhere²⁶. The structural consequences of rigidity percolation in glassy networks appear to have a common theme. The present results on Si-Te glasses and those reported recently on Ge-Se and As-Ge-Se glasses suggest that at or above the mechanical threshold, the elastically rigid domains largely derive from crystal-like molecular fragments.

The present experiments also show that oxygen impurity atoms readily alloy in both the rigid and floppy fragments of $\text{Si}_x\text{Te}_{1-x}$ glass network. In the former instance the large increase in both T_g 's and T_c 's upon alloying presumably arises because impurity atoms terminate edges of Te chains. In the latter instance oxygen impurity atoms are localized at specific defects sites of the rigid fragment, thus frustrating crystallization of the glass to realize $c\text{-Si}_2\text{Te}_3$.

6. ACKNOWLEDGEMENTS

We thank Dr. S. Asokan and collaborators for useful correspondence. The work at the University of Cincinnati was supported by grant DMR-85-21005 from the National Science Foundation.

7. REFERENCES

1. Richard Zallen, The Physics of Amorphous Solids, John Wiley & Sons New York 1983 provides a good overview; also see J.C. Phillips in The Structure of Non-Crystalline Materials 1982, Taylor and Francis, Inc. New York 1983 pp. 123-136.
2. K. Murase, T. Fukunaga, K. Yakushiji, T. Yoshimi and I. Yunoki, *J. Non Cryst. Solids* 59-60, 883-888 (1983).
3. P.H. Gaskell in Glassy Metals II, pp. 5-49 H. Beck and H.J. Guntherodt ed. (Springer: Berlin) (1984).
4. P. Boolchand in Physical Properties of Amorphous Systems, pp. 221-260, David Adler, Brian B. Schwartz and Martin C. Steele, ed. Plenum Press, New York (1985).
5. J.C. Phillips, J.C. Bean, B.A. Wilson and A. Ourmazd, *Nature* 325, 121-125 (1987).
6. R.N.ENZWEILER and P. Boolchand, *Solid State Commun.* 62(3), 197-200 (1987). Also see P. Boolchand, *Comments Cond. Mat. Phys.* 12(4), 163-180 (1986).
7. M. Tenhover, M.A. Hazle and R.K. Grasselli, *Phys. Rev. Lett.* 51, 404-408 (1983); J.E. Griffiths, M. Malyj, G.P. Espinosa and J.P. Remeika, *Phys. Rev. B* 30(12), 6978-90 (1984).
8. R.W. Johnson Ph.D. Thesis, University of Chicago 1986; Also see S. Susman et al. in Defects in Glasses, pp. 91-99 Frank L. Galeener, David L. Griscom, Marvin J. Weber ed, Materials Research Society Vol. 6, Pittsburg (1986). S.R. Elliot (private commun.)
9. P. Boolchand in Defects in Glasses, pp. 57-74, Frank L. Galeener, David L. Griscom, Marvin J. Weber ed, Materials Research Society, Vol. 61, Pittsburg (1986).
10. J. Cornet in Structure and Properties of Non Crystalline Semiconductors pp. 72-77, B.T. Kolomiets ed., Academy of Sciences of the USSR, (1975).
11. G. Dittmar and H. Schafer *Acta Crystallogr. Sect. B* 32, 2726-29 (1976).
12. P.E. Gregoriades, G.L. Bleris and J. Stoemenos, *Acta Cryst.* B39, 421-426 (1983).
13. J.C. Phillips, *J. Non. Cryst. Solids* 34, 153-181 (1979) and 43, 37-77 (1981).
14. M. Thorpe, *J. Non. Cryst. Solids* 57, 355-375 (1983).
15. Argon Gas UN1006; Ultra High Purity Grade, Linde Specialty Gas.
16. J.E. Griffiths, G.P. Espinosa, J.P. Remeika and J.C. Phillips, *Phys. Rev.* B25, 1272-1291 (1982).
17. P. Boolchand, B.B. Triplett, S.S. Hanna and J.P. deNeufville in Mössbauer Effect Methodology, Vol. 9 pp. 53-80, Plenum Press New York (1974).
18. S. Asokan, G. Parthasarathy and E.S.R. Gopal, *J. Non. Cryst. Solids* 86, 48-64 (1986).
19. B. Norban, D. Persing, R.N.ENZWEILER, P. Boolchand, J.E. Griffiths and J.C. Phillips, *Phys. Rev. B* (in press).
20. M.B. Meyers and E.J. Felty, *Mat. Res. Bull.* 2, 535-547 (1967).
21. J. Grothaus and P. Boolchand, *J. Non. Cryst. Solids* 72, 1-22 (1985).
22. A.S. Pine and G. Dresselhaus, *Phys. Rev.* B4, 356-368 (1971).
23. K. Ziegler, H. Junker and U. Birkholz, *Phys. Stat. Solid A* 37, K-79-81 (1976). Also see reference 12.
24. M. Malyj, G.P. Espinosa and J.E. Griffiths, *Phys. Rev.* B31, 3672-79 (1985).
25. P. Boolchand *Hyperfine Interactions* 27, 3-14 (1986).
26. S. Asokan, G. Parthasarathy and E.S.R. Gopal, *Phys. Rev.* B35, 8269-8272 (1987).